Multicarrier-signal design with low peaks and low out-of-band power

Miguel Ángel Vázquez Oliver

Department of Electrical and Information Technology
Lund University

Advisor: Thomas Magesacher

September 16, 2009

Printed in Sweden
E-huset, Lund, 2009

Abstract

The high peak-to-average power ratio (PAPR) and the high out-of-band power (OBP) are two major drawbacks of multicarrier communication systems. Many PAPR reduction and OBP supression techniques have been proposed in the literature whereas not much has been proposed regarding the jointly reduction performance. This thesis focuses on joint reducing time-domain peaks and out-of-band leakage of OFDM signals. The resulting algorithm combines the benefits of both methods and yields better results than each method does separately.

Acknowledgment

First and foremost I would like to thank my thesis advisor Thomas Magesacher, who has shown a large and consistent interest in my project during the times. His many constructive comments have greatly improved this work. He is also thanked for his patience for answering all my questions during his time in Stanford.

Most of the thesis work was done while I was exchange student at Lunds Tekniska Högskola in Lund. It is a pleasure to thank the Electrical and Information Technology department for their hospitality. I am also indebted to the many people in Lund in and outside the department who made my stay in Sweden a very pleasant one.

My final words go to my parents. They have always supported and encouraged me to do my best in all matters of life. To them I dedicate this thesis

Table of Contents

Chapter 1
Introduction

Multicarrier transmission, also known as orthogonal frequency-division modulation (OFDM), a technique that has been invented a long time ago [1, 2], has recently seen rising popularity in wireless and wireline applications. The recent interest in this technique is mainly due to the recent advances in digital signal processing technology which rendered the implementation of OFDM feasible. International standards making use of OFDM for high-speed wireless communications are already established or being established by IEEE 802.20, and the European Telecomunications Standards Institute (ETSI) Broadcast Radio Acces Network (BRAN) committees. For wireless applications, an OFDM-based system can be of interest because it provides greater immunity to multipath fading and impulse noise, and eliminates the need for long time domain equalizers, while the DFT operation can be implemented efficiently in hardware using fast Fourier transform (FFT) techniques.

One of the major drawbacks of multicarrier transmission is the high peak-to-average power ratio (PAPR) of the transmit signal. If the peak transmit power is limited by either regulatory or application-related constraints, the admissible average power of a multicarrier signal is a way below the average power of transmit signal generated by constant-modulus modulation. This in turn reduces the range of multicarrier transmission. Especially for low-cost applications, the drawback of high PAPR may outweigh all the potential benefits of multicarrier transmission systems.

Another potential drawback (depending on the scenario) of OFDM systems is the high out-of-band power (OBP) due to the sidelobes of the subcarriers. A high OBP of the system can lead to significant interference with the legacy system and therefore has to be reduced. Another scenario where high OBP can be problematic is the uplink of a cellular network using orthogonal frequency division multiple acces (OFDMA). In such a system, each user is assigned a small block of subcarriers. Since the oscillators of mobiles are not synchronized, and due to different Doppler shifts, the signals arrive with different frequency offsets at the base station and the orthogonality between the subcarriers is lost. The resulting multiple acces interference can be reduced by minimizing the OBP of all signals.

A number of approaches have been proposed to deal with the PAPR and OBP problems. However, not much it has been published about minimizing both parameters simultaneously. In this thesis, it is proposed to use a set of reserved tones that are modulated such that both PAPR and the OBP are reduced. This

work is mainly based on [5] and [10] where each of them suffer from the other one: the PAPR reduction method presented in [10] increases the OBP and the OBP supression method [5] suffers from a high PAPR. The simulation results presented show the superior performance of the joint optimization.

The thesis is structured as follows. Chapter 2 gives an overview of the OFDM system, presents the PAPR and the Power Spectral Density notion and introduces the notation that will be used throughout the paper. Chapter 3 reviews the algorithm which this work is based on as well as other approaches which have been proposed to mitigate both problems separately. Chapter 4 focuses on the proposal of the joint optimization algorithm. In chapter 5, simulation results are presented that show the performance of the algorithm. The summary in chapter 6 concludes the thesis.

Chapter 2
Background

2.1 Multicarrier modulation

To send information over a finite-length channel, the data is partitioned into blocks of bits, and each block is mapped into a vector of complex symbols $\mathbf{X}^m = \left[X_0^m \cdots X_{N-1}^m\right]^T$. The modulated waveform $\mathbf{x}^m$ is

$$\mathbf{x}^m = \sum_{k=0}^{N-1} \mathbf{m}_k X_k^m = M\mathbf{X}^m \tag{2.1}$$

where $\{\mathbf{m}_k, k = 0, \ldots, N-1\}$ denotes the set of transmit basis vectors and M is the matrix constructed with the transmit basis vectors as its columns. At the receiver, the received vector $\mathbf{y}^m$ is demodulated by computing

$$\mathbf{Y}^m = \begin{bmatrix} \mathbf{f}_0^T \mathbf{y}^m \\ \vdots \\ \mathbf{f}_{N-1}^T \mathbf{y}^m \end{bmatrix} = F\mathbf{y}^m \tag{2.2}$$

where $\{\mathbf{f}_k, k = 0, \ldots, N-1\}$ denote the set of receive basis vectors and F is the matrix constructed with the receive basis vectors as its rows. The overall input-output relation is given by

$$\mathbf{Y}^m = FHM\mathbf{X}^m + F\mathbf{n} \tag{2.3}$$

where H is defined to have the *(i,j)th* entry as h_{i-j} and where $\mathbf{n}$ is the received noise vector. $h = \begin{bmatrix} h_0 & h_1 & \ldots & h_L \end{bmatrix}$ is the impulse response of the channel.

$$H = \begin{bmatrix} h_0 & 0 & 0 & \ldots & 0 \\ \vdots & h_0 & 0 & \ldots & 0 \\ h_L & \ldots & \ddots & \ldots & \vdots \\ \vdots & \ddots & \ldots & \ddots & 0 \\ 0 & \ldots & h_L & \ldots & h_0 \end{bmatrix} \tag{2.4}$$

Different choices for F and M are possible, leading to a number of possible multicarrier structures. For non-trivial channels, a variety of multicarrier structures have been proposed, each with a different choice of basis vectors. By means

of maximizing the Signal-to-Noise Ratio (SNR), it has been shown in [11] that the best option is to choose F and M which diagonalize the channel matrix. However, this approach requires complete knowledge of the channel. Because of this, Vector Coding, which is the name of this modulation, is usually not found in practical applications.

Instead of the Singular Value Decomposition (SVD) of the channel, another approach can be applied. It can be shown that, with a slight modification of the channel matrix, the DFT basis functions can obtain as good results as the Vector Coding technique. The next section will introduce the most popular DFT-based multicarrier modulation: OFDM.

2.2 Orthogonal Frequency Division Multiplexing (OFDM)

In order to split the information into N parallel streams, OFDM forces the modulated transmit vector $\mathbf{x}^m$ to satisfy the constraint

$$x^m_{-k} = x^m_{N-k}, \quad k = 1, \ldots, M \quad \forall m \tag{2.5}$$

Replicating the last M samples at the beginning of the symbol is called cyclic prefix insertion. By adding a cyclic prefix, the resulting channel matrix can be written as

$$\hat{H} = \begin{bmatrix} h_0 & 0 & \ldots & 0 & h_M & \ldots & h_1 \\ h_1 & h_0 & \ddots & & 0 & \ddots & \vdots \\ \vdots & h_1 & & \ddots & \ddots & \ddots & h_M \\ h_M & \vdots & \ddots & \ddots & & & 0 \\ 0 & h_M & & \ddots & \ddots & & \vdots \\ \vdots & \ddots & \ddots & & \ddots & \ddots & \vdots \\ 0 & \ldots & 0 & h_M & & h_1 & h_0 \end{bmatrix} \tag{2.6}$$

where the channel matrix $\hat{H}$ is $N \times N$ circulant matrix. For this special case, the SVD of $\hat{H}$ is much simpler to compute.

The Discrete Time Fourier Transform (DFT) of an N-dimensional vector $\mathbf{w} = \begin{bmatrix} w_0 & \ldots w_{N-1} \end{bmatrix}^T$ is also an N-dimensional vector $\mathbf{W} = \begin{bmatrix} W_0 & \ldots W_{N-1} \end{bmatrix}^T$ with the components given by

$$W_k = \frac{1}{\sqrt{N}} \sum_{n=0}^{N-1} w_n e^{-j\frac{2\pi}{N}kn}, \quad k = 0, \ldots, N-1 \tag{2.7}$$

Similarly, the Inverse Discrete Fourier Transform (IDFT) is given by

$$w_k = \frac{1}{\sqrt{N}} \sum_{n=0}^{N-1} W_n e^{j\frac{2\pi}{N}kn}, \quad k = 0, \ldots, N-1 \tag{2.8}$$

Equivalently, the DFT and IDFT can be written in matrix form as

$$\mathbf{W} = Q\mathbf{w} \tag{2.9}$$

$$\mathbf{w} = Q^*\mathbf{W} \tag{2.10}$$

where Q is the unitary DFT matrix with elements $q_{k,n} = \frac{1}{\sqrt{N}} e^{-j\frac{2\pi}{N}kn}$ and Q^* is the IDFT matrix. Using this notation, it has been shown in [16] that the circulant matrix $\hat{H}$ has eigen-decomposition

$$\hat{H} = Q^*\Lambda Q \tag{2.11}$$

where Λ is a diagonal matrix with the elements $\lambda_k = H_k = DFT(\mathbf{h})$ on its main diagonal. Thus, choosing the columns of Q^* as transmit basis vectors, i.e. $M = Q^*$, and the rows of Q as receive basis vectors, i.e. $F = Q$, the input-output relationship can be written as

$$Y_k^m = H_k X_k^m + N_k^m, \quad k = 0, \ldots, N-1 \tag{2.12}$$

The channel is partitioned into independent Additive White Gaussian Noise (AWGN) channels and thus making the receiver much simpler.

The main advantage of the OFDM structure compared to the standard Vector Coding, is that the DFT can be implemented with order $\mathcal{O}(N\log N)$ operations instead of N^2 operations for a general matrix multiplication. Therefore, transmitter ($\mathbf{x}^m = Q^*\mathbf{X}^m$) and receiver ($\mathbf{Y}^m = Q\mathbf{y}^m$) can be implemented very efficiently. The penalty to be paid for this large reduction in complexity is a slight performance degradation with respect to Vector Coding due to the cyclic prefix restriction.

This thesis assumes multicarrier modulation with a long-enough cyclic prefix to ensure diagonalization of the channel.

2.3 OFDM signals

An OFDM transmit signal is the sum of N, independent, Quadrature-Amplitude-Modulated (QAM) sub-signals or tones, each with equal bandwidth and frequency separation $1/T$, where T is the time duration of the OFDM symbol. The continuous-time baseband representation of a single multicarrier symbol is given by

$$x^m(t) = \frac{1}{\sqrt{N}} \sum_{k=0}^{N-1} X_k^m e^{-j\frac{2\pi}{T}kt} w(t), \tag{2.13}$$

where m is the symbol index, $w(t)$ is a rectangular window (nominally of height 1 over the interval $[0, T]$) and X_k^m is the QAM value of the k-th symbol or tone. As explained in the previous section, to simplify the equalizer design in the presence of finite-length dispersion in time, OFDM systems insert a cyclic prefix before every OFDM symbol. The equalizer then becomes a simple scaling as long as the duration of the combined effect of the channel multipath propagation plus transmit and receiver filtering is shorter than the length of the CP, T_{CP}. The cyclic prefix is simply a periodic extension of the symbol over the interval $[-T_{\mathrm{CP}}, 0]$ resulting in a symbol of length $[-T_{\mathrm{CP}}, T]$. Then the previous equation becomes

$$x_{\mathrm{CP}}^m(t) = \frac{1}{\sqrt{N}} \sum_{k=0}^{N-1} X_k^m e^{-j\frac{2\pi}{T}kt} w_{\mathrm{CP}}(t), \tag{2.14}$$

where $w_{\mathrm{CP}}(t)$ is a rectangular window of height one over the interval $[-T_{\mathrm{CP}}, T]$. For continuous data transmission, the transmitter sends these symbols sequentially:

$$x_{\mathrm{C}}(t) = \sum_{m=-\infty}^{\infty} x_{\mathrm{CP}}^{m}(t - m(T_{\mathrm{CP}} + T)). \tag{2.15}$$

This transmit signal is not bandlimited due to the $\mathrm{sinc}(f(T+T_{\mathrm{CP}}))$ behaviour exhibited by the rectangular windowing function $w_{\mathrm{CP}}(t)$, and is typically followed by a filter. Moreover, with this representation, computing $x_{\mathrm{C}}(t)$ requires the calculation of a Fourier Series, which is very hard to implement with analog components and can only be approximated with digital hardware. Therefore in practise, complex baseband OFDM signals are typically generated by using the Inverse Discrete Fourier Transform as described in Figure 2.1. The *m-th* block of encoded bits

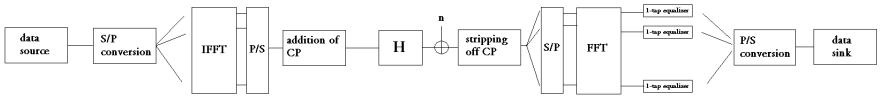

Figure 2.1: Structure of an orthogonal-frequency-division-multiplexing transmission chain with cyclic prefix and one-tap equalization

is mapped into the complex-valued OFDM vector of QAM constellation points $\mathbf{X}^m = [X_0^m \dots X_{N-1}^m]^T$, which is then transformed via an IDFT into the T/N-spaced discrete-time vector $\mathbf{x}^m = [x_0^m \dots x_{N-1}^m]^T = IDFT(\mathbf{X}^m)$, i.e.

$$x^m[n] = \frac{1}{\sqrt{N}} \sum_{k=0}^{N-1} X_k^m e^{-j\frac{2\pi}{T}kn} w[n] \tag{2.16}$$

where $w[n]$ is the discrete-time rectangular window of height one over the interval $[0, N]$.

2.4 Peak-to-Average-Power Ratio (PAPR)

One of the major problems of OFDM is that the peak amplitude of the emitted signal can be considerably higher than the average amplitude. This *Peak-to-Average-Power Ratio* (PAPR) issue originates from the fact that an OFDM signal is the superposition of N sinusoidal signals with different frequencies. On average the emitted power is linearly proportional to N. However, sometimes, the signals on the subcarriers add up constructively, so that the amplitude of the signal is proportional to N, and the peak power is proportional to N^2.

Since all practical transmission systems are peak-power limited, designing a system to operate in a perfectly linear region often implies operating at average

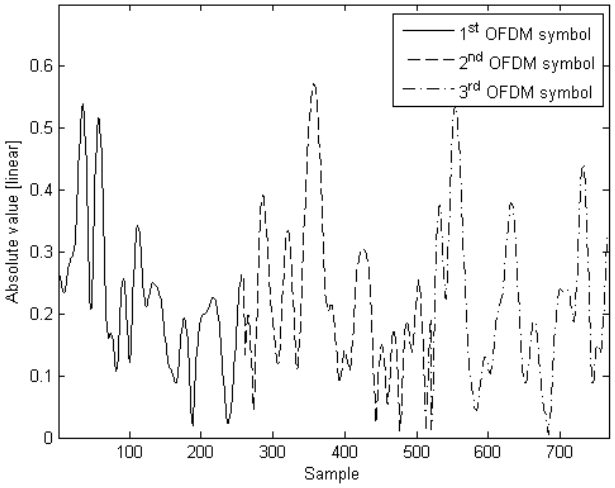

Figure 2.2: Three consecutive OFDM symbols. $N = 16$

power levels way below the maximum power available. In practice, to avoid operating the amplifiers with extremely large back-offs, occasional saturation of the power amplifiers or clipping in the Digital-to-Analog Converters (DAC) must be allowed. This additional nonlinear distorsion creates inter-modulation distorsion that increases the bit error rate in standard linear recievers, and also causes spectral widening of the transmit signal which can lead to adjacent-channel interference to other users.

Typically the PAPR is used to quantify the envelope excursions of the signal. The PAPR of a signal x_τ where τ is used to represent both the continuous-time index n and discrete-time index t, is defined as:

$$PAPR\{\mathbf{x}_\tau\} = \frac{[\|\mathbf{x}_\tau\|_\infty]^2}{E\{|\mathbf{x}_\tau|^2\}} \tag{2.17}$$

Here, $\|\mathbf{x}_\tau\|_\infty$ denotes the infinity norm (maximum instantaneous power), $E\{|\mathbf{x}_\tau|^2\}$ denotes the average power of the signal and $\tau \in T$ is the interval over which the PAPR is evaluated.

2.5 Out-of-band power emission

Since an OFDM signal is a cyclostacionary process, the Power Spectral Density (PSD) is given by

$$PSD(f) = \sum_m r(m) e^{-j2\pi fm} \tag{2.18}$$

where $r(m)$ is the averaged autocorrelation sequence

$$r(m) = \frac{1}{N} \sum_{n=n_0}^{n_0+N-1} r(n,m) \tag{2.19}$$

where $r(n,m)$ is the autocorrelation sequence given by

$$r(n,m) = E[\mathbf{x}[n]\mathbf{x}^*[n-m]], \quad n,m = -\infty, \ldots, \infty \tag{2.20}$$

Assuming the data is uncorrelated over each block, it can be shown that the resulting PSD of a single active carrier is given by

$$\frac{1}{N}|W_k(f)|^2 \tag{2.21}$$

where $W_k(f)$ is the Fourier transform of the time limited k-th carrier. If the data is uncorrelated over each carrier, the resulting PSD is the sum of all carriers. Otherwise, the PSD needs to be calculated according to (2.18).

Essentially, an OFDM signal consists of a number of unfiltered QAM carriers. As a result, the out-of-band spectrum decreases rather slowly, according to a sinc function. For a larger number of subcarriers, the spectrum goes down more rapidly in the beginning, which is caused by the fact that the sidelobes are closer together. However, even the spectrum for 256 carriers has a relatively large -40 dB bandwith that is almost four times the -3 dB bandwidth.

Chapter 3

Review of the research

3.1 PAPR reduction techniques

3.1.1 Amplitude clipping and filtering

The simplest technique for PAPR reduction might be amplitude clipping [6]. Amplitude clipping limits the peak envelope of the input signal to a predetermined value or otherwise passes the input signal through unperturbed, that is,

$$\begin{cases} x, & |x| \leq A \\ Ae^{j\phi(x)} & |x| > A \end{cases} \tag{3.1}$$

where $\phi(x)$ is the phase of x. The distorsion caused by amplitude clipping can be viewed as another source of noise. The noise caused by amplitude clipping appears both in-band and out-band. In-band distorsion cannot be reduced by filtering and results in an error performance degradation, while out-of-band radiation reduces spectral efficiency. Filtering after clipping can reduce out-of-band radiation but may also cause some peak regrowth so that the signal after clipping and filtering will exceed the clipping levels at some points. To reduce overall peak regrowth, a repeated clipping-and-filtering operation can be used [7, 8]. Generally, repeated clipping-and-filtering takes many iterations to reach a desired amplitude level. When repeated clipping-and-filtering is used in conjunction with other PAPR reduction techniques, the deleterious effects may be significaly reduced.

There are a few techniques proposed to mitigate the harmful effects of the amplitude clipping. In [21], a method to iteratively reconstruct the signal before clipping is proposed. This method is based on the fact that the effect of clipping noise is mitigated when decisions are made in frequency domain. When the decisions are converted back to the time domain, the signal is recovered somewhat from the harmful effects of clipping, although this may not be perfect. An improvement can be made by repeating the above procedures. Another way to compensate for the performance degradation from clipping is to reconstruct the clipped samples based on the other samples in the oversampled signals. In [22], oversampled signal reconstruction is used to compensate for SNR degradation due to the clipping for low values of clipping threshold. In [23], iterative estimation and cancellation of clipping noise is proposed. This technique exploits the fact

that clipping noise is generated by a known process that can be recreated at the receiver and subsequently removed.

3.1.2 Coding

Coding can also be used to reduce the PAPR. A simple idea introduced in [24] is to select those codewords that minimize or reduce the PAPR for transmission.

However, this approach suffers from the need to perform an exhaustive search to find the best codes and to store large lookup tables for encoding and decoding, especially for a large number of subcarriers. Moreover, this approach does not address the problem of error correction. A more sophisticated approach proposed in [25] is to use the codewords drawn from offsets generated by a linear code. The idea is to choose the code for its error correcting properties and the offset to reduce the PAPR of the resulting coded signals. This approach enjoys the twin benefits of PAPR reduction and error correction, and is simple to implement, but it requires extensive calculation to find good codes and offsets. A computationally efficient geometrical approach to offset selection is introduced in [26], but there is no guarantee about the amount of PAPR reduction that can be obtained with this approach.

On the other hand, it is discovered that the use of a Golay complementary sequence [27] as codewords to control the modulation results in signals with PAPR of at most two. It is found in [28] that the large set of binary length 2^m Golay complementary pairs can be obtained from certain second-order cosets of the classical first-order Reed-Muller code. Thus, it is possible to combine the block coding approach (with all of the encoding, decoding and error correcting capability) and the use of Golay complementary sequences (with their attractive PAPR control properties).

Considering that the usefulness of these techniques is limited to multicarrier systems with a small number of subcarriers and the required exhaustive search for good codes is intractable, the actual benefits of coding for PAPR reduction for practical multicarrier systems are limited.

3.1.3 The partial transmit sequence technique

In the Partial Transmit Sequence (PTS) technique, an input data block of N symbols is partioned into disjoint subblocks. The subcarriers in each subblock are weighted by a phase factor for that subblock. The phase factors are selected such that the PAPR of the combined signal is minimized. Figure 3.1 shows the block diagram of the PTS technique. In the ordinary PTS technique [29, 30], the input data block $\mathbf{X}$ is partioned into $\mathcal{M}$ disjoint subblocks $\mathbf{X}_m = [X_{m,0}, X_{m,1}, \ldots, X_{m,N-1}]^T, \quad m = 1, 2, \ldots, \mathcal{M}$, such that $\sum_{m=1}^{\mathcal{M}} \mathbf{X}_m = \mathbf{X}$ and the subblocks are combined to minimize the PAPR in the time domain. The L-times oversampled time domain signal of $\mathbf{X}_m, m = 1, 2, \ldots, \mathcal{M}$, is denoted $\mathbf{x}_m = [x_{m,0}, x_{m,1}, \ldots, x_{m,NL-1}]^T$. $\mathbf{x}_m, m = 1, 2, \ldots, \mathcal{M}$, is obtained by taking the IDFT of length NL on $\mathbf{X}_m$ concatenated with $(L-1)N$ zeros. These are called the partial transmit sequences. Complex phase factors, $b_m = e^{j\phi_m}, m = 1, 2, \ldots, \mathcal{M}$, are introduced to combine the PTSs. The set of phase factors is denoted as vector

$\mathbf{b} = [b_1, b_2, \ldots, b_{\mathcal{M}}]^T$. The time domain signal after combining is given by

$$\mathbf{x}'(\mathbf{b}) = \sum_{m=1}^{M} b_m \mathbf{x}_m \tag{3.2}$$

where $\mathbf{x}'(\mathbf{b}) = [x'_0(\mathbf{b}), x'_1(\mathbf{b}), \ldots, x'_{NL-1}(\mathbf{b})]^T$. The objective is to find the set of phase factors that minimizes the PAPR. Minimization of PAPR is related to the minimization of

$$\max_{0 \le k \le NL-1} |x'_k(\mathbf{b})| \tag{3.3}$$

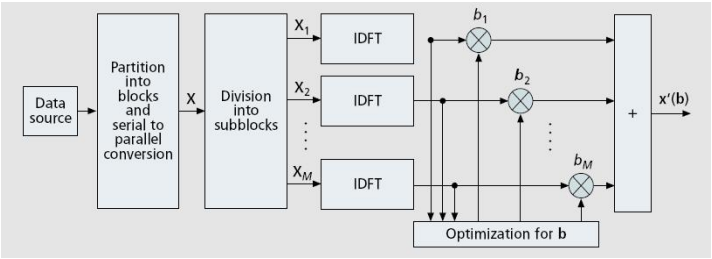

Figure 3.1: A block diagram of the PTS technique

In general, the selection of the phase factors is limited to a set with a finite number of elements to reduce the search complexity. The set of allowed phase factors is written as $P = e^{j2\pi/Wl} | l = 0, 1, \ldots, W-1$, where W is the number of allowed phase factors. In addition, we can set $b_1 = 1$ without any loss of performance. So, it is convenient to perform an exhaustive search for M phase factors. Hence, $W^{\mathcal{M}-1}$ sets of phase factors are searched to find the optimum set of phase factors. The search complexity increases exponentially with the number of subblocks $\mathcal{M}$. PTS needs $\mathcal{M}$ IDFT operations for each data block, and the number of required side information bits is $\lfloor \log_2 W^{\mathcal{M}-1} \rfloor$, where $\lfloor y \rfloor$ denotes the largest integer that does not exceed y. The amount of PAPR reduction depends on the number of subblocks $\mathcal{M}$ and the number of allowed phase factors $W-1$. Another factor that may affect the PAPR reduction performance in PTS is the subblock partitioning, which is the method of division of the subcarriers into multiple disjoint subblocks. There are three kinds of subblock partitioning schemes: adjacent, interleaved, and pseudo-random partitioning [30]. The PTS technique works with an arbitrary number of subcarriers and any modulation scheme.

3.1.4 The selected mapping technique

In the Selected Mapping Technique (SLM) technique, the transmitter generates a set of sufficiently different candidate data blocks, all representing the same information as the original data block, and selects the most favorable for transmission [31]. A block diagram of the SLM technique is shown in Figure 3.2. Each data block is multiplied by U different phase sequences, each of length N, $\mathbf{B}^{(u)} = [b_{u,0}, b_{u,1}, \ldots, b_{u,N-1}]^T, \quad u = 1, 2, \ldots, U$, resulting in U modified data blocks. To

include the unmodified data block in the set of modified data blocks, we set $\mathbf{B}^{(1)}$ as the all-one vector of length N. Let us denote the modified data block for the u-th phase sequence $\mathbf{X}^{(u)} = [X_0 b_{u,0}, X_1 b_{u,1}, \ldots, X_{N-1} b_{u,N-1}]^T, u = 1, 2, \ldots, U$. After applying SLM to $\mathbf{X}$, the multicarrier signal becomes

$$x^{(u)}(t) = \frac{1}{\sqrt{N}} \sum_{n=0}^{N-1} X_n b_{u,n} e^{j2\pi n \Delta f t}, \quad 0 \le t \le NT, \quad u = 1, 2, \ldots, U \tag{3.4}$$

Among the modified data blocks $\mathbf{X}^{(u)}, u = 1, 2, \ldots, U$, the one with the lowest PAPR is selected for transmission. Information about the selected phase sequence should be transmitted to the receiver as side information. At the receiver, the reverse operation is performed to recover the original data block. For implementation, the SLM technique needs U IDFT operations, and the number of required side information bits is $\lfloor \log_2 U \rfloor$ for each data block. This approach is applicable with all types of modulation and any number of subcarriers. The amount of PAPR reduction for SLM depends on the number of phase sequences U and the design of the phase sequences.

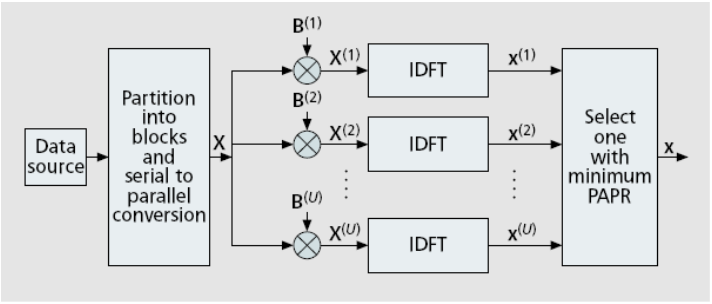

Figure 3.2: A block diagram of the SLM technique

3.1.5 The interleaving technique

The interleaving technique for PAPR reduction is very similar to the SLM technique. In this approach, a set of interleavers is used to reduce the PAPR of the multicarrier signal instead of a set of phase sequences [32]. An interleaver is a device that operates on a block of N symbols and reorders or permutes them; thus, data block $\mathbf{X} = [X_0, X_1, \ldots, X_{N-1}]^T$ becomes $\mathbf{X}' = [X_{\pi(0)}, X_{\pi(1)}, \ldots, X_{\pi_{(N-1)}}]^T$ where $\{n\} \leftrightarrow \{\pi(n)\}$ is a one-to-one mapping $\pi(n) \in \{0, 1, \ldots, N-1\}$ and for all n. To generate K modified data blocks, interleavers are used to produce permuted versions of a given data block. The PAPR of K permuted data blocks and that of the original data block are computed using K IDFT operations; the data block with the lowest PAPR is then chosen for transmission. To recover the original data block, the receiver needs know which interleaver is used at the transmitter; thus, the number of required side information bits is $\lfloor \log_2 K \rfloor$. Both the transmitter and receiver store the permutation indices $\{\pi(n)\}$ in memory. Thus, interleaving and deinterleaving can be done simply. The amount of PAPR reduction depends on the number of interleavers K and the design of the interleavers.

3.1.6 Tone reservation

The Tone reservation (TR) method is based on adding a data-block-dependent time domain signal to the original signal to reduce its peaks. This time domain signal can be easily computed at the transmitter and stripped off at the receiver.

The transmitter does not send data on a small subset of of subcarriers. Instead, these subcarriers are used to maximize PAPR reduction [10]. The objective is to find the time domain signal to be added to the original time domain $\mathbf{x}$ such that the PAPR is reduced. If we add a frequency domain vector $\mathbf{C} = [C_0, C_1, \ldots, C_{N-1}]^T$ to $\mathbf{X}$, the new time domain signal can be represented as $\mathbf{x} + \mathbf{c} = IDFT\{\mathbf{X} + \mathbf{C}\}$, where $\mathbf{c}$ is the time domain signal due to $\mathbf{C}$. The TR technique restricts the data block $\mathbf{X}$ and peak reduction vector $\mathbf{C}$ to lie in disjoint frequency subspaces. The L nonzero positions in $\mathbf{C}$ are called peak reduction carriers (PRCs). Since the subcarriers are orthogonal, these additional signals cause no distorsion on the data-bearing subcarriers. To find the value of C_n, it is necessary to solve a convex optimization problem that, in the DMT case, can easily be cast as a linear programming (LP) problem.

In the case of DMT for wireline systems, there are typically subcarriers with SNRs too low for sending information, so these subcarriers must go unused and are available for PAPR reduction. In wireless systems, however, there is often no fast reliable channel state feedback to dictate which subcarriers can be used for PAPR reduction without significant loss of throughput. Instead, a set of subcarriers must be reserved regardless of received SNRs, resulting in a bandwidth sacrifice.

3.2 Out-of-band power reduction

3.2.1 Windowing

To make the spectrum decay more rapid, windowing can be applied to the individual OFDM symbols. Windowing an OFDM symbol makes the amplitude go smoothly to zero at the symbol boundaries. A commonly used window type is the raised cosine window.

In practice, the OFDM signal is generated as follows: first, N_c input QAM values are padded with zeros to get N input samples that are used to calculate an IFFT. Then, the last T_{prefix} samples of the IFFT output are inserted at the start of the OFDM symbol, and the first T_{postfix} samples are appended at the end. The OFDM symbol is then multiplied by a raised cosine window $w(t)$ to more quickly reduce the power of out-of-band carriers. The OFDM symbol is then added to the previous OFDM symbol with a delay of T_s, such that there is an overlap region of βT_s, where β is the roll-off factor of the raised cosine window.

3.2.2 Filtering

Instead of windowing, it is also possible to use conventional filtering techniques to reduce the out-of-band spetrum. Windowing and filtering are dual techniques; multiplying an OFDM symbol by a window corresponds to a convolution of the spectrum of the window function with a set of impulses at the carriers frequencies.

When filtering is applied, a convolution is done in the time domain and the OFDM spectrum is multiplied by the frequency response of the filter. When using filters, care has to be taken not to introduce rippling effects on the envelope of the OFDM symbols over a timespan that is larger than the roll-of region of the windowing approach. Too much rippling means the undistorted part of the OFDM envelope is smaller, and this directly translates into less delay spread tolerance. Notice that digital filtering techniques are more complex to implement than windowing. A digital filter requires at most a few multiplications per sample, while windowing only requires at least a few multiplications per symbol, for those samples which fall into the roll-off region. Hence, because only a few percent of the samples are in the roll-off region, windowing is an order of magnitude less complex than digital filtering.

3.2.3 Spectral compensation

In the same way as tone reservation for PAPR reduction, spectral compensation divides the N tones into two sets: a set S_c of compensation tones and a set S_i of information tones, which occupy disjoint frequency bins. The transmitter modulates each compensation tone with a linear combination of the data transmitted over a set of compensation tones. Using properly chosen tones as compensation tones leads to a better exploitation of the spectral mask in the sense that the power on some of the information tones can be increased [13]. Spectral compensation does not require any shaping-related processing at the receiver: simple tone-wise equalization is possible since the orthogonality of the received basis functions is preserved. Consequently, the technique conforms with any standard.

3.2.4 K-continuous OFDM

Most techniques focus on frequency-domain measures while K-continuous OFDM focuses on continuity in time-domain [9]. In this technique, it is changed the correlation of modulation symbols between consecutive OFDM symbols by forcing the OFDM signal to be continuous at the transition time instants. K-continuous OFDM does not exhibit sensitivity to the length of the cyclic prefix. More importantly, this approach accomplishes significant supression even at distant frequencies, where the effect of the spectral compensation is limited.

Chapter 4
Problem formulation

Sections 4.1 and 4.2 describe methods based on tone reservation techniques. All these structures can be formulated as:

$$\bar{x}^m[n] = x^m[n] + c^m[n] = \frac{1}{\sqrt{N}} \sum_{k=0}^{N-1} (X_k^m + C_k^m) e^{j\frac{2\pi}{N}kn} \tag{4.1}$$

where the frequency vector $\mathbf{C}^m = [C_0^m \dots C_{N-1}^m]^T$ or equivalenty, the time domain sequence $c^m[n]$ are the reduction signals. Since not all the carriers are reserved and in order to simplify the notation, it is defined a diagonal carrier selection matrix S by

$$S_{ii} = \begin{cases} 1 & \text{if carrier } i \text{ is reserved tone} \\ 0 & \text{otherwise} \end{cases} \tag{4.2}$$

Now, it is possible to rewrite 4.1 as

$$\bar{x}^m[n] = x^m[n] + c^m[n] = \frac{1}{\sqrt{N}} \sum_{k=0}^{N-1} (X_k^m + S_{kk} C_k^m) e^{-j\frac{2\pi}{N}kn} \tag{4.3}$$

It is assumed that X_k just contains the data carriers, the other reserved frequency bins are 0-valued.

4.1 PAPR reduction via tone reservation

As it has been explained in section 2.4, the definition of the PAPR is

$$PAPR\{\bar{\mathbf{x}}^m\} = PAPR\{\mathbf{x}^m + \mathbf{c}^m\} = \frac{[\|\mathbf{x}^m + \mathbf{c}^m\|_\infty]^2}{E\{|x^m[n]|^2\}} \tag{4.4}$$

Since the denominator is not a function of the PAPR reduction signals, the problem of minimizing the PAPR of the combined signal is equivalent to computing the value of $\mathbf{c}^{m,[\text{opt}]}$, or equivalently $\mathbf{C}^{m,[\text{opt}]}$, that minimizes the maximum peak value or the infinity norm of $\mathbf{x}^m + \mathbf{c}^m$. That is,

$$\min_{\mathbf{c}} \|\mathbf{x}^m + \mathbf{c}^m\|_\infty = \min_{\mathbf{C}} \|x^m + QS\mathbf{C}^m\|_\infty \tag{4.5}$$

which can be reformulated as

$$\begin{aligned} \min_{\mathbf{C}} \quad & t \\ \text{subject to} \quad & \|\mathbf{x}^m + QS\mathbf{C}^m\|_\infty \leq t \end{aligned} \tag{4.6}$$

The above problem is convex since it minimizes a linear function over an intersection of quadratic (and thus convex) constraints in the variables $\mathbf{C}$. Specifically, this is a special case of a Quadratically Constrained Quadratic Program (QCQP) which is a well-studied problem and has a convex formulation.

4.2 Out-of-band power reduction

In order to reduce the out-of-band emission, the objective function will require that the 0th-order and a few higher-order derivatives are continuous at the transition time instant between the m-th and (m-1)-th OFDM symbol.

$$\frac{\mathrm{d}^l}{\mathrm{d}t^l}\bar{x}^m(t)\bigg|_{t=-T_G} = \frac{d^l}{dt^l}\bar{x}^{m-1}(t)\bigg|_{t=T_s} \tag{4.7}$$

for all $m \geq 1$ and for $l = 0, 1, \ldots, K$. For OFDM symbols given by (4.3), the characterization (4.7) becomes

$$\sum_{k\in\mathcal{C}} k^l e^{j\phi k}\bar{\mathbf{X}}_k^m = \sum_{k\in\mathcal{C}} k^l \bar{\mathbf{X}}_k^{m-1} \tag{4.8}$$

where $\mathcal{C}$ is the set of carriers, $k \in \mathcal{C} = \{k_0, k_1, \ldots, k_{N-1}\}$ and $\phi = -2\pi\frac{T_g}{T_s}$. An equivalent vectorized form of this characterization is

$$A\Phi\bar{\mathbf{X}}^m = A\bar{\mathbf{X}}^{m-1} \tag{4.9}$$

where, naturally, $\bar{\mathbf{X}}^m = \mathbf{X}^m + S\mathbf{C}^m$ while $\Phi = \mathrm{diag}(e^{j\phi k_0}, e^{j\phi k_1}, \ldots, e^{j\phi k_{N-1}})$ and

$$A = \begin{pmatrix} k_0^0 & k_1^0 & \ldots & k_{N-1}^0 \\ k_0^1 & k_1^1 & \ldots & k_{N-1}^1 \\ \vdots & \vdots & & \vdots \\ k_0^K & k_1^K & \ldots & k_{N-1}^K \end{pmatrix} \tag{4.10}$$

It is possible to find an analytical solution for (4.9), however, it was observed that the unconstrained optimization problem sometimes yields a solution that assigns much more power to the reserved tones than to the corresponding number of data carriers. In order to avoid this problem, power constraints are incorporated into the optimization algorithm.

$$\begin{aligned} \min_{C} \quad & \|A\Phi\bar{\mathbf{X}}^m - A\bar{\mathbf{X}}^{m-1}\|_2 \\ \text{subject to} \quad & \|C_k\|_2 \leq \gamma_k \quad \forall k \in \mathcal{C}_r \end{aligned} \tag{4.11}$$

where $\mathcal{C}_r$ is the subset of reserved carriers.

4.3 Joint reduction

Equations (4.11) and (4.6) are two optimization problems for the reduction of the out-of-band power and peak-to-average power ratio, respectively. In order to achieve a joint reduction of both values, both criteria are combined to yield the vector-valued objective function

$$f_0(\mathbf{C}) = \begin{bmatrix} t \\ \|A\Phi\bar{\mathbf{X}}^m - A\bar{\mathbf{X}}^{m-1}\|_2 \end{bmatrix} \tag{4.12}$$

In general, there does not exist an optimal value C^* for the multicriterion problem $\min_C f_0(C)$ (i.e. a vector C^* that simultaneously minimizes both the PAPR and the OBP). Therefore, the problem is scalarized by multiplying it with the weighting vector $[1 - \beta\mu\beta]$. The trade-off parameter $\beta \in [0, 1]$ determines the relative weighting of the two optimization criteria. Varying β yields the set of Pareto optimal points, i.e., the optimal trade-off curve in the (PAPR, OBP)-reduction plane. The purpose of the factor μ is given by

$$\mu = \frac{\|\mathbf{x}\|_\infty}{\|A\Phi\mathbf{X}^m - A\bar{\mathbf{X}}^{m-1}\|_2} \tag{4.13}$$

is to ensure that the two optimization criteria are approximately equally weighted for a value of $\beta = 0.5$. The total optimization problem can now be stated as follows:

$$\begin{aligned} \min_C \quad & \begin{bmatrix} 1-\beta \\ \mu\beta \end{bmatrix}^T \begin{bmatrix} t \\ \|A\Phi\bar{\mathbf{X}}^m - A\bar{\mathbf{X}}^{m-1}\|_2 \end{bmatrix} \\ \text{subject to} \quad & \|C_k\|_2 \leq \gamma_k \quad \forall k \in \mathcal{C}_r \\ & \|x^m + QS\mathbf{C}^m\|_\infty \leq t \end{aligned} \tag{4.14}$$

Since the objective function as well as both constraint functions are convex, (4.14) is a convex optimization problem and can hence be solved by standard algorithms like the gradient descent method or Newton's method. Note that these algortihms always converge to the global optimum due to the convexity of the problem [18].

Chapter 5
Simulation results

In this section, simulation results are presented showing the performance of the joint optimization algorithm. The results have been obtained using `CVX`, a package for specifying and solving convex programs [19, 20].

An OFDM system with 256 subcarriers is considered where 64 of them are activated $(97, 98, \ldots, 158, 159)$ and where 48 of them are in use. The carriers $\{96, 104, \ldots, 152, 160\}$ are chosen as reserved tones. An analysis of the optimum positions of the reserved tones, was outside the focus of this work; however, in [5] it is stated that spreading the reserved tones over the available bandwidth yields better performance than, for example, with clustered reserved tones.

The power allocated to each reserved tone is not limited, the purpose of this is to show the performance of the algorithm when the reserved tones employ the power what they need. $K = 1, 2, 3$, which means, according to (4.11), that the OFDM symbols are equalized till the $0^{th}, 1^{st}, 2^{nd}$ derivative, respectively. The simulation parameters are summarized in Table 5.1.

In order to quantify the performance of the reduction algorithm, both the PAPR and OBP of the signal with optimized reserved tones are compared to a reference signal where the reserved tones are randomly QPSK modulated, i.e. serve as normal data carriers.

Table 5.1: Simulation Parameters

FFT-length	$N = 64$
Length of CP	$M = 4$
Alphabet	QPSK
Used Subcarriers	$\mathcal{C} = \{97, 98, \ldots, 158, 159\}$
Reserved Tones	$\mathcal{C}_r = \{96, 104, \ldots, 152, 160\}$
Oversampling Factor	$L = 4$
Derivative to be equalized	$K = 0, 1, 2$
Power constraint	$\gamma = \infty$dB

Fig. 5.1 shows the mean reduction of both quantities as a function of the trade-off parameter β. In the first case, $K = 0$, there is no variation: the residual norm remains equal to zero and the PAPR is not reduced and equal 0.48 dB in average.

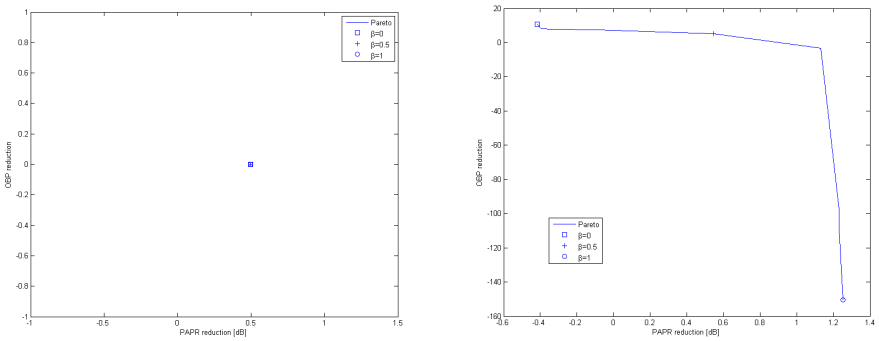

(a) $K = 0$ **(b)** $K = 1$

Figure 5.1: Pareto curves $K = 0, 1 \quad |\mathcal{C}_r| = 8$

Then, when the 1^{st} derivative is equalized, the achievable PAPR reduction is around 0.4 dB for $\beta = 0$, and increases to about 1.2 dB as more emphasis is put on to the OBP reduction. Thus, a pure OBP reduction even leads to slight PAPR increase. On the other hand, the OBP reduction reaches a maximum of more than 150 [linear] for $\beta = 1$[1]. An erratic behaviour is shown in the third case which is due to the high power levels reached by the reserved tones.

So far, only the mean performance has been considered. To give an idea of the distribution of the PAPR and OOB values, CCDF and PSD are observed. The CCDFs plots show the complementary cumulative distribution function[2] (CCDF) of PAPR of different optimizations varying β and PSD plots show the Power Spectral Density[3] (PSD) for the same β values as well as for the reference signal without any reserved tones.

In the first case, as it has been seen in Fig. 5.1a, there is no variation in the results when β is modified. However, when more derivatives are equalized, it is possible to distinguish the effect of the variation of the trade-off parameter. In both cases, $K = 1$ and $K = 2$, the drawback of separately optimizing PAPR or OOB can be observed: when exclusively reducing the PAPR ($\beta = 0$) the OOB increases. In the same way, when exclusively reducing the OBP ($\beta = 1$) the PAPR increases . Moreover, when the trade-off parameter does not have an extreme value, the reserved tones which are located at the edge of the used spectra yield unacceptable power levels. In spite of this, it is shown in Fig. 5.6 how the PAPR is increased in every β step. On the contrary, in Fig. 5.8 shows a random behaviour of the PAPR reduction. Although not fully investigated yet, the most likely explanation

[1] The OBP reduction is calculated as the value of the norm (4.11) after the optimization

[2] The CCDF of the PAPR denotes the probability that a data block exceeds a given threshold.

[3] The power spectrum is estimated using the Welch's averaged periodogram method with a 33-sample Hanning window and a 32-sample overlap. Moreover, the signal consists in 1000 OFDM symbols.

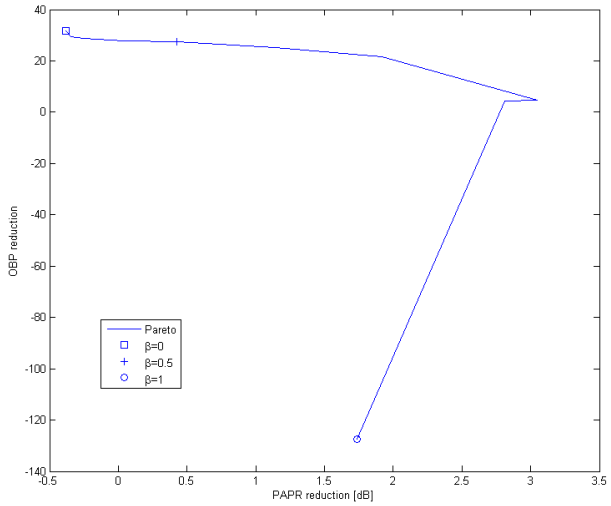

Figure 5.2: Pareto curve $K = 2, \quad |\mathcal{C}_r| = 8$

for the randomness is probably the high power levels of the reserved tones. Notice that this phenomen was also shown in the trade-off curve Fig. 5.2.

Let us now consider a more realistic scenario. Simulation results are presented for an 802.11a compliant OFDM system in which 48 carriers of 64 are used [14]. Futhermore, the reserved tones are constrained using the specifications of the standard which means, according to the mathematical model depicted in (4.14), $\gamma_k = m_k \quad \forall k \in \mathcal{C}_r$ where $\mathbf{m}$ is a mask constructed taking into account the standard 802.11a Fig 5.9 . Moreover, the reserved tones are clustered at the edges of the spectrum. Table 5.2 summarizes the new simulation parameters.

Table 5.2: Simulation parameters

FFT-length	$N = 64$
Length of CP	$M = 4$
Alphabet	QPSK
Used subcarriers	$\mathcal{C} = \{104, 105, \ldots, 151, 152\}$
Reserved tones	$\mathcal{C}_r = \{96, 97, \ldots, 159, 160\}$
Oversampling factor	$L = 4$
Derivative order	$K = 0, 1, 2$
Power constraint	$\gamma_k = m_k$

Fig. 5.10, Fig. 5.12 and Fig. 5.15 show the effect of the power constraint: the reserved tones do not exceed the mask in any case. Again, when just the continuity is equalized, there is no noticable variation when β is changed. Because

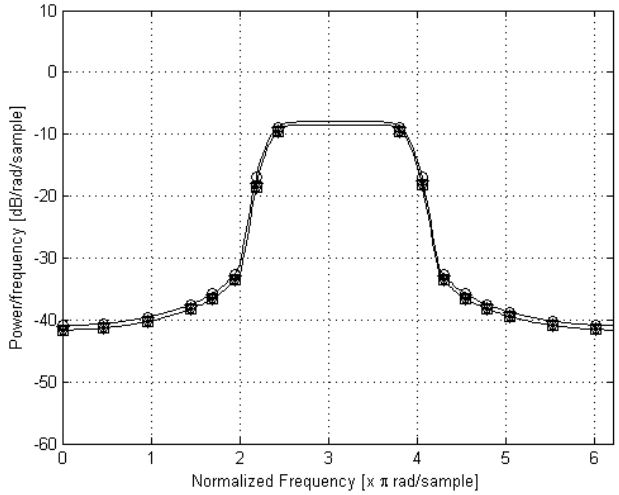

Figure 5.3: PSD $K = 0, \quad |\mathcal{C}_r| = 8.$ ∘:Plain OFDM, $\times : \beta = 0, \quad * : \beta = 0.25, \quad \square : \beta = 0.5, \quad \diamond : \beta = 0.75, \quad \bigtriangledown : \beta = 1.$

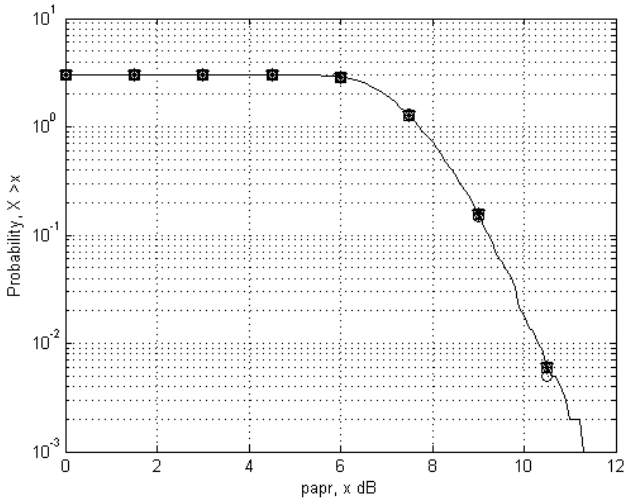

Figure 5.4: CCDF $K = 0, \quad |\mathcal{C}_r| = 8.$ ∘:Plain OFDM, $\times : \beta = 0, \quad * : \beta = 0.25, \quad \square : \beta = 0.5, \quad \diamond : \beta = 0.75, \quad \bigtriangledown : \beta = 1.$

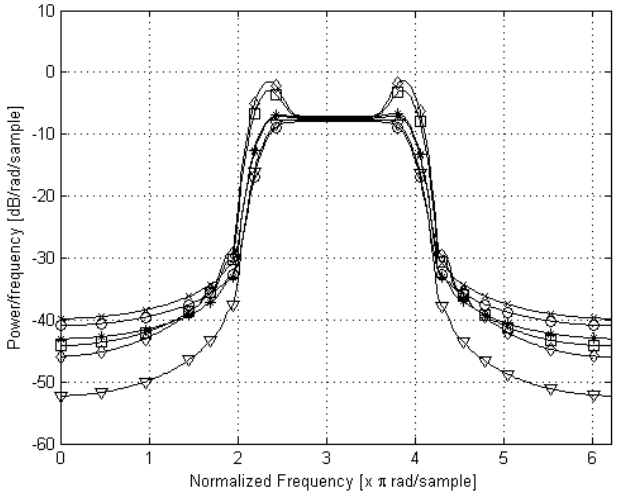

Figure 5.5: PSD $K = 1, \quad |\mathcal{C}_r| = 8.$ ∘:Plain OFDM, $\times : \beta = 0, \quad * : \beta = 0.25, \quad \square : \beta = 0.5, \quad \diamond : \beta = 0.75, \quad \bigtriangledown : \beta = 1.$

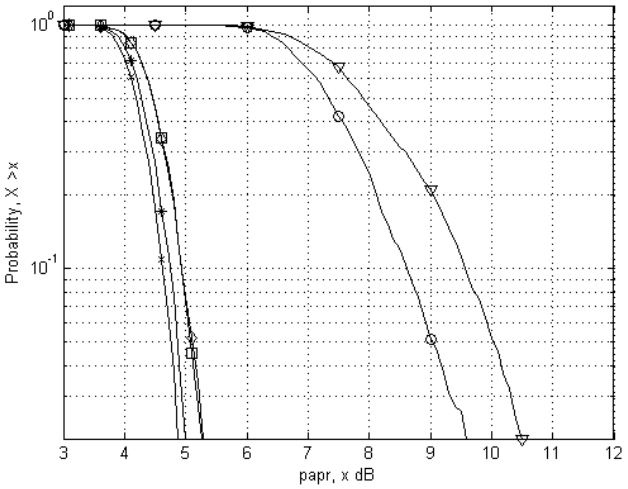

Figure 5.6: CCDF $K = 1, \quad |\mathcal{C}_r| = 8.$ ∘:Plain OFDM, $\times : \beta = 0, \quad * : \beta = 0.25, \quad \square : \beta = 0.5, \quad \diamond : \beta = 0.75, \quad \bigtriangledown : \beta = 1.$

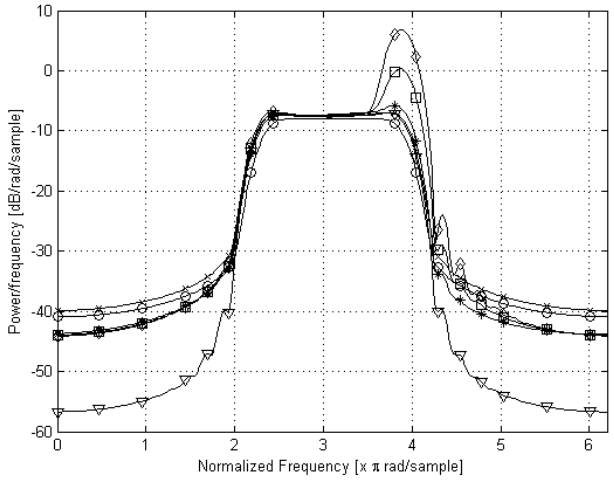

Figure 5.7: PSD $K = 2$, $|\mathcal{C}_r| = 8$. ∘:Plain OFDM, $\times : \beta = 0$, $* : \beta = 0.25$, $\square : \beta = 0.5$, $\diamond : \beta = 0.75$, $\bigtriangledown : \beta = 1$.

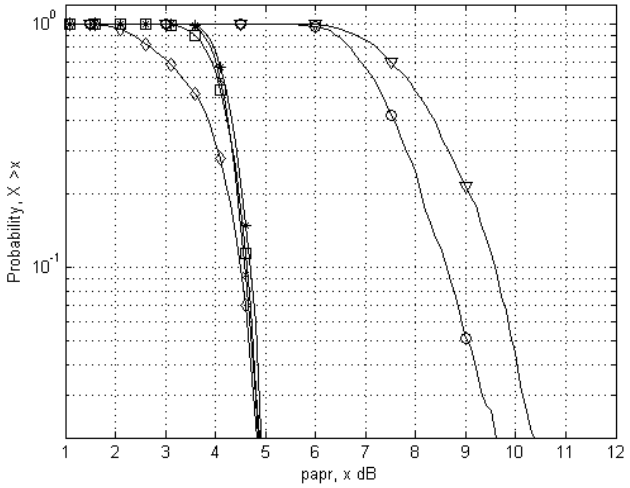

Figure 5.8: CCDF $K = 2$, $|\mathcal{C}_r| = 8$. ∘:Plain OFDM, $\times : \beta = 0$, $* : \beta = 0.25$, $\square : \beta = 0.5$, $\diamond : \beta = 0.75$, $\bigtriangledown : \beta = 1$.

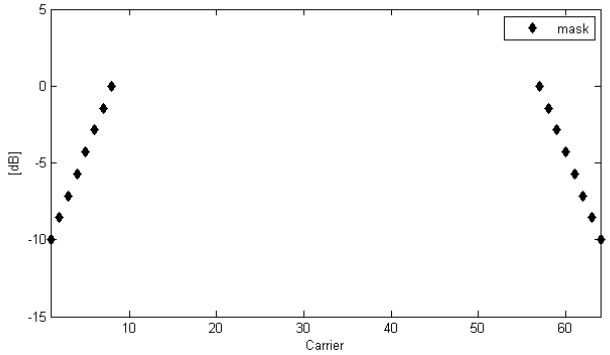

Figure 5.9: 802.11a spectral mask ○:Plain OFDM, $\times$: $\beta = 0$, $*$: $\beta = 0.25$, $\square$: $\beta = 0.5$, $\diamond$: $\beta = 0.75$, $\bigtriangledown$: $\beta = 1$.

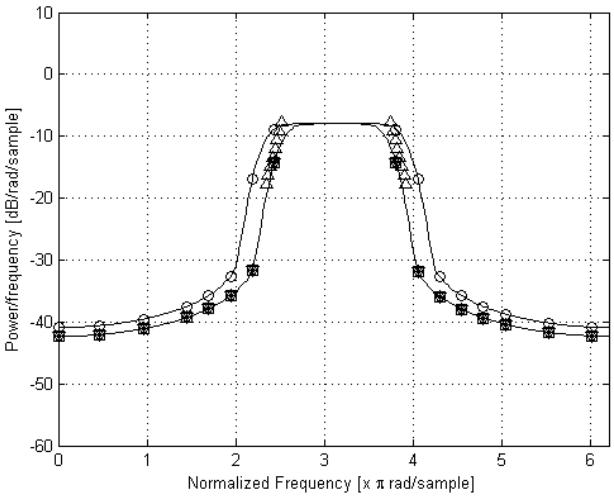

Figure 5.10: PSD of 802.11a scenario $K = 0$, $|\mathcal{C}_r| = 16$ ○:Plain OFDM, $\times$: $\beta = 0$, $*$: $\beta = 0.25$, $\square$: $\beta = 0.5$, $\diamond$: $\beta = 0.75$, $\bigtriangledown$: $\beta = 1$.

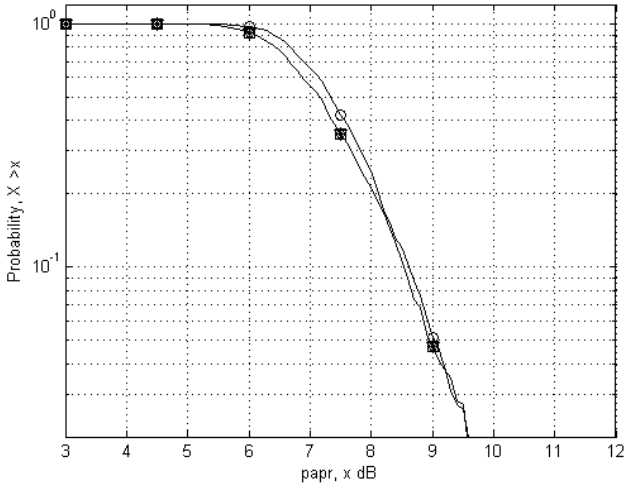

Figure 5.11: CCDF of 802.11a scenario $K = 0$, $|\mathcal{C}_r| = 16$ ○:Plain OFDM, $\times : \beta = 0$, $* : \beta = 0.25$, $\square : \beta = 0.5$, $\diamond : \beta = 0.75$, $\bigtriangledown : \beta = 1$.

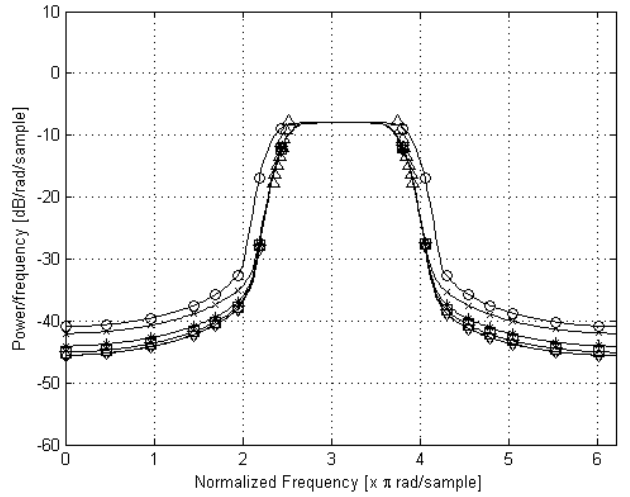

Figure 5.12: PSD of 802.11a scenario $K = 1$, $|\mathcal{C}_r| = 16$ ○:Plain OFDM, $\times : \beta = 0$, $* : \beta = 0.25$, $\square : \beta = 0.5$, $\diamond : \beta = 0.75$, $\bigtriangledown : \beta = 1$.

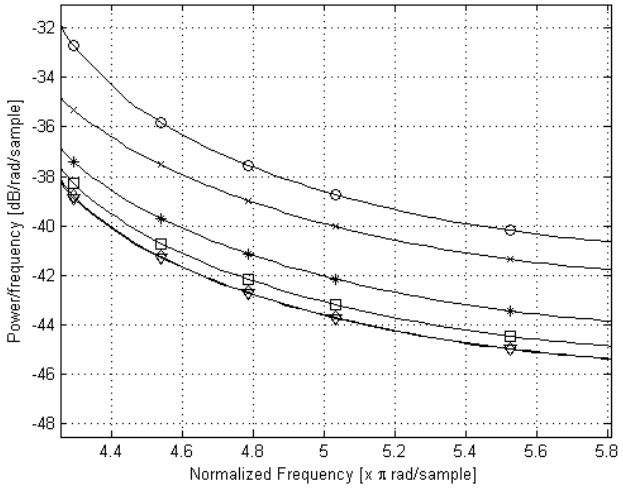

Figure 5.13: PSD of 802.11a scenario (detail) $K = 1$, $|\mathcal{C}_r| = 16$ ∘:Plain OFDM, $\times : \beta = 0$, $* : \beta = 0.25$, $\square : \beta = 0.5$, $\diamond : \beta = 0.75$, $\bigtriangledown : \beta = 1$.

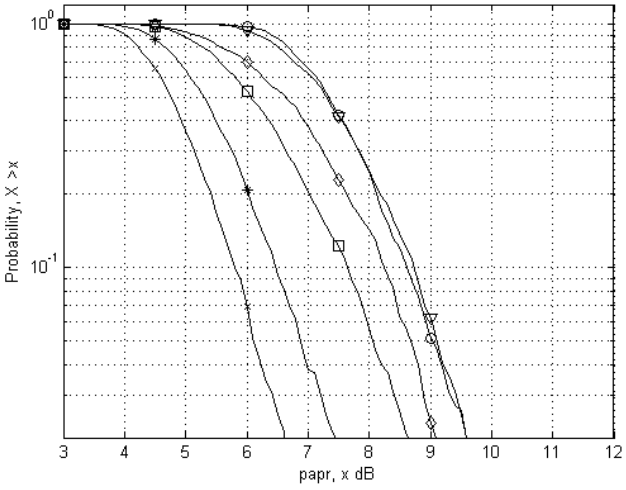

Figure 5.14: CCDF of 802.11a scenario $K = 1$, $|\mathcal{C}_r| = 16$ ∘:Plain OFDM, $\times : \beta = 0$, $* : \beta = 0.25$, $\square : \beta = 0.5$, $\diamond : \beta = 0.75$, $\bigtriangledown : \beta = 1$.

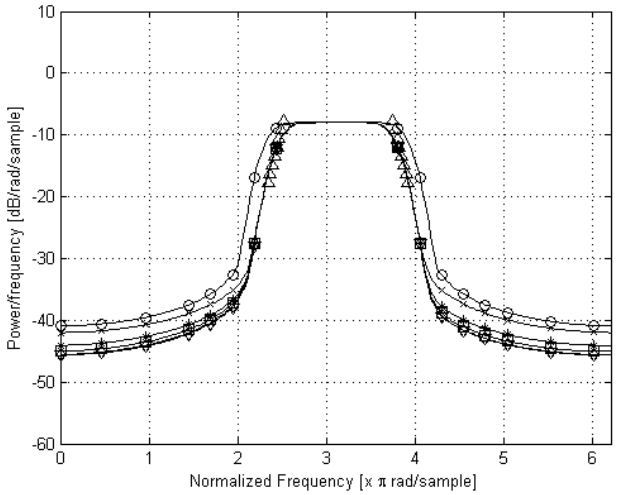

Figure 5.15: PSD of 802.11a scenario $K = 2$, $|\mathcal{C}_r| = 16$ ○:Plain OFDM, $\times : \beta = 0$, $* : \beta = 0.25$, $\square : \beta = 0.5$, $\diamond : \beta = 0.75$, $\bigtriangledown : \beta = 1$.

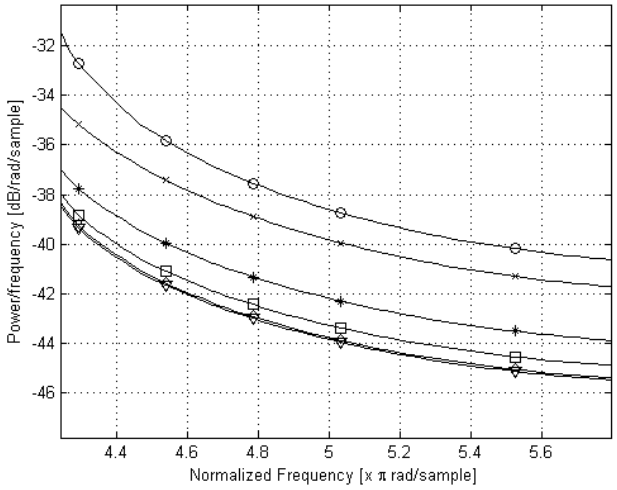

Figure 5.16: PSD of 802.11a scenario (detail) $K = 2$, $|\mathcal{C}_r| = 16$ ○:Plain OFDM, $\times : \beta = 0$, $* : \beta = 0.25$, $\square : \beta = 0.5$, $\diamond : \beta = 0.75$, $\bigtriangledown : \beta = 1$.

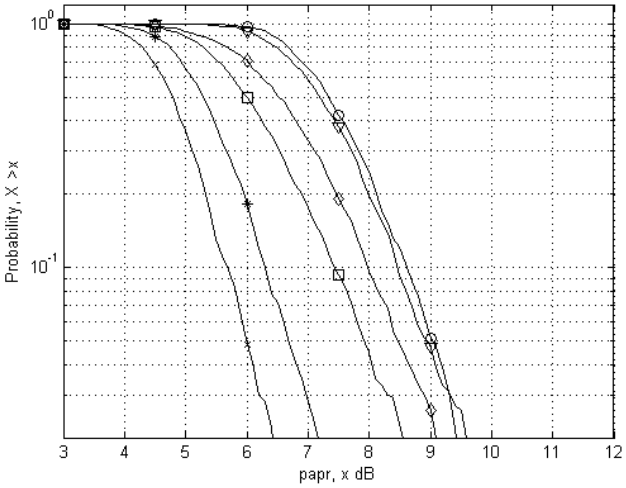

Figure 5.17: CCDF of 802.11a scenario $K = 2$, $|\mathcal{C}_r| = 16$ ○:Plain OFDM, $\times$: $\beta = 0$, $*$: $\beta = 0.25$, $\square$: $\beta = 0.5$, $\diamond : \beta = 0.75$, $\bigtriangledown : \beta = 1$.

of the power limitation in the reserved tones, the PAPR is much lower in this case, Fig. 5.11.

The joint reduction algorithm yields a better performance for $K = 1$ and $K = 2$. Since the spectra do not have that high peaks, the method performs a more soft reduction in both cases. Moreover, it is appreciated a high variation in PAPR when β is changed in CCDFs graphics, Fig. 5.14 and Fig 5.17.

Chapter 6
Conclusions

It has been proposed to use the tone reservation technique, which has been examined in the literature separately for peak-to-average power ratio reduction and out-of-band power reduction, in order to jointly optimize both PAPR and OBP. Simulation results show the superior performance of the joint reduction in comparison to a system that performs just one of the methods. A further advantage is the possibility to adjust the relative weighting of the two criteria dynamically. The joint reduction approach is therefore a promising technique for OFDM systems in which both a high PAPR and a high OBP are problematic, as for example in cellular mobile systems with an OFDMA-based uplink.

For a real-time implementation of the proposed algorithm, however, its relatively high computational complexity has to be considered. Therefore, algorithms with lower complexity will be investigated in future work.

References

[1] R.W. Chang, *Synthesis of Band Limited Orthogonal Signals for Multichannel Data Transmission.* Bell Sys. Tech. J. pp. 1775-1796 December 1966.

[2] B. R. Saltzberg, *Performance of an Efficient Parallel Data Transmission System.* IEEE Trans. Commun, pp. 805-811 December 1967.

[3] Richard Van Nee, Ramjee Prasad, *OFDM for wireless multimedia communications.* Artech House Publishers, Boston, London 1st Edition, 2000.

[4] Andreas F. Molisch, *Wireless communications.* John Wiley & Sons, Southern Gate, Chichester, 1st Edition, 2006.

[5] J. Van de Beek and F.Breggren, *Out-of-band power supression in OFDM.* IEEE Commun. Letters, pp. 609-611 September 2008.

[6] R. O'Neill and L. B. Lopes, *Envelope variations and spectral splatter in clipped multicarrier signals.* Proc. IEEE PIMRC'95, Toronto, Canada, pp. 71-75 September 1995.

[7] X. Li and L. J. Cimini Jr., *Effect of clipping and filtering on the performance of OFDM.* IEEE Commun. Letters, pp. 131-133 May 1998.

[8] J. Amstrong, *Peak-to-average power reduction for OFDM by repeated clipping and frequency domain* . Elec. Letters, pp. 246-247 February 2002.

[9] J. Van de Beek and F.Breggren, *N-continuous OFDM.* IEEE Commun. Letters, pp. 1-3 January 2009.

[10] Jose Tellado-Mourelo, *Peak to average power reduction for multicarrier modulation.* PhD dissertation, September 1999.

[11] J. M. Cioffy, *Advanced digital communication.* Course reader, Stanford University 2008-2009.

[12] Thomas Magesacher, *Spectrum efficiency in OFDMA.* January 2009.

[13] Thomas Magesacher, *Spectral compensation for multicarrier communication.* IEEE Transaction on Sig. Proc. pp. 3366-3379 July 2007.

[14] *Wireless LAN medium access control (MAC) and physical layer (PHY) specifications: High-speed physical layer in the 5 Ghz Band*, IEEE Std. 802.11a, September. 1999.

[15] M. Senst, M. Jordan, M. Dörpinghaus, M. Färber, G. Ascheid, and H. Meyr, *Joint Reduction of Peak-to-Average Power Ratio and Out-of-Band Power in OFDM Systems*. IEEE Commun. Letters, pp. 3812-3816 November 2007.

[16] Zhengdao Wang and Georgios B. Giannakis, *Wireless Multicarrier Communications, where Fourier meets Shannon*. IEEE Magazine of Sig. Proc. pp. 29-48 May 2000.

[17] S. H. Han and J. H. Lee, *An overview of peak-to-average power ratio reduction techniques for multicarrier transmission*. IEEE Wireless Commun. Magazine. pp. 56-65 April 2005.

[18] S.Boyd and L. Vandenberghe, *Convex Optimization*. Cambridge University Press, 2004.

[19] M. Grant and S. Boyd. *CVX: Matlab software for disciplined convex programming* (web page and software). http://stanford.edu/~boyd/cvx, June 2009.

[20] M. Grant and S. Boyd. Graph implementations for nonsmooth convex programs, *Recent Advances in Learning and Control (a tribute to M. Vidyasagar)*, V. Blondel, S. Boyd, and H. Kimura, editors, pages 95-110, *Lecture Notes in Control and Information Sciences*, Springer, 2008. http://stanford.edu/~boyd/graph_dcp.html.

[21] D. Kim and G. L. Stüber, *Clipping noise mitigation for OFDM by decision-aided reconstruction*. IEEE Commun. Letters pp. 4-6 January 1999.

[22] H. Saeedi, M. Sharif, and F. Marvasti, *Clipping noise cancellation in OFDM systems using oversampled signal reconstruction*. IEEE Commun. Letters pp. 73-75 February 2002.

[23] H. Chen and M. Haimovish, *Iterative estimation and cancellation of clipping noise for OFDM signals*. IEEE Commun. Letters pp. 305-307 July 2003.

[24] A. E. Jones and T. A. Wilkinson, and S. K. Barton, *Block coding scheme for reduction of peak to mean envelope power ratio of multicarrier transmission scheme*. Elec. Letters pp. 2098-2099 December 1994.

[25] A. E. Jones and T. A. Wilkinson, *Combined coding for error control and increased robustness to system nonlinearities in OFDM*. Proc IEEE VTC'96 pp. 904-908 May 1996.

[26] V. Tarokh and H. Jafarkhani, *On the computation and reduction of the peak-to-average power ratio in multicarrier communications*. IEEE Trans. Commun. pp. 37-44 January 2000.

[27] M. Golay, *Complementary series*. IEEE Trans. Info Theory pp. 82-87 April 1961.

[28] J. A. Davis and J. Jedwad, *Peak-to-mean power control and error correction for OFDM transmission using Golay sequences and Reed-Muller Codes*. Elect. Letters pp. 267-268 February 1997.

[29] S. H. Müller and J. B. Huber, *OFDM with reducted peak-to-average power ratio by optimum combination of partial transmit sequences.* Elect. Letters pp. 368-369. February 1997.

[30] S. H. Müller and J. B. Huber, *A novel peak power reduction scheme for OFDM.* Proc. IEEE PIMRC'97 pp. 1090-1094. September 1997.

[31] R. W. Bäuml, R. F. H. Fisher, and J. B. Huber, *Reducting the peak-to-average power ratio of multicarrier modulation by selected mapping.* Elect. Letters pp. 2056-2057 October 1996.

[32] G. R. Hill, M. Faulkner, and J. Singh, *Reducting the peak-to-average power ratio of multicarrier modulation by cyclically shifting partial transmit sequences.* Elect. Letters pp. 560-561 March 2000.